

First-principles Landau-like potential for BiFeO₃ and related materials

Natalya S. Fedorova,^{1,*} Dmitri E. Nikonov,² Hai Li,² Ian A. Young,² and Jorge Íñiguez^{1,3,†}

¹*Materials Research and Technology Department,
Luxembourg Institute of Science and Technology,*

5 Avenue des Hauts-Fourneaux, L-4362 Esch/Alzette, Luxembourg

²*Components Research, Intel Corporation, Hillsboro, 97124 Oregon, USA*

³*Department of Physics and Materials Science, University of Luxembourg, 41 Rue du Brill, L-4422 Belvaux, Luxembourg*

In this work we introduce the simplest, lowest-order Landau-like potential for BiFeO₃ and La-doped BiFeO₃ as an expansion around the paraelectric cubic phase in powers of polarization, FeO₆ octahedral rotations and strains. We present an analytical approach for computing the model parameters from density functional theory. We illustrate our approach by computing the potentials for BiFeO₃ and La_{0.25}Bi_{0.75}FeO₃ and show that, overall, we are able to capture the first-principles results accurately. The computed models allow us to identify and explain the main interactions controlling the relative stability of the competing low-energy phases of these compounds.

I. INTRODUCTION

Magnetoelectric multiferroics, materials that simultaneously show magnetic and electric orders, are of significant interest, since the coexistence and coupling of these orders hold great potential for development of multifunctional devices^{1,2}. BiFeO₃ is among the most exciting and extensively studied representatives of this family because it displays both orders at room temperature³.

Ferroelectricity appears in BiFeO₃ at $T_C \sim 1100$ K^{4,5}. Below T_C , it has a rhombohedrally distorted perovskite structure (space group $R3c$, #161)^{6,7}, which differs from the perfect cubic phase by the presence of two distortions: (i) polar displacements of Bi³⁺ and Fe³⁺ cations with respect to O²⁻ anions (Bi³⁺ dominates due to its stereochemically active 6s lone pairs⁸) giving rise to a spontaneous polarization \mathbf{P} of up to 100 $\mu\text{C}/\text{cm}^2$ along a pseudocubic $\langle 111 \rangle$ direction^{9,10}; and (ii) antiphase rotations \mathbf{R} of the FeO₆ octahedra about the same pseudocubic $\langle 111 \rangle$ direction as the polarization ($a^- a^- a^-$ in Glazer's notation¹¹)^{12,13}. (In the following, all directions are in the pseudocubic setting.)

Below $T_N \sim 640$ K, BiFeO₃ also shows G-type antiferromagnetic (G-AFM) order with the nearest-neighbor Fe spins antialigned^{4,14}. The canting of the Fe spins driven by Dzyaloshinskii-Moriya (DM) interaction^{15,16} can give rise to a weak magnetization in this material. The DM interaction relies on the symmetry breaking caused by the FeO₆ octahedral tilts of BiFeO₃¹²; indeed, the phase of the octahedral rotations defines the sign of the DM vector and, in turn, that of the weak magnetization. In bulk BiFeO₃ an incommensurate cycloidal spiral is superimposed on the G-AFM order, yielding a zero net magnetization¹⁷. This cycloid, however, can be suppressed by doping in bulk systems¹⁸ and by epitaxial constraints in BiFeO₃ films¹⁹⁻²². Therefore, ferroelectricity can coexist with weak ferromagnetism in BiFeO₃ at ambient conditions.

Additionally, a 180° deterministic switching of the DM vector and weak magnetization by an electric field has been reported from a combined experimental and

theoretical study of BiFeO₃ films grown on DyScO₃ substrates²². It is proposed that the magnetoelectric switching is the result of a peculiar polarization reversal that is found to occur in two steps, a 109° rotation followed by a 71° rotation (or *vice versa*); further, the FeO₆ octahedral tilts are believed to reverse together with the polarization, resulting in the observed reversal of the weak magnetic moment. Note that octahedral tilts will typically not follow polarization in a single-step 180° reversal and, therefore, a two-step switching path is crucial for controlling the weak magnetization in BiFeO₃ by an electric field. These observations make BiFeO₃ a promising candidate for applications in magnetoelectric memory elements. However, to be technologically relevant, switching characteristics have to be optimized such that coercive voltages are below 100 mV and switching times fall in the range of 10-1000 ps^{23,24}. Hence, the current challenge is to optimize the ferroelectric switching in BiFeO₃ while retaining the two-step path and magnetoelectric control.

One of the efficient strategies for optimizing polarization switching in BiFeO₃ is doping by La. Indeed, since polarization in this compound largely originates from the 6s lone pairs of the Bi³⁺ cations, their substitution by isovalent, lone-pair-free cations leads to a reduction of the polar distortion^{3,25,26}. For example, it has been experimentally demonstrated that 15-20% La-doped BiFeO₃ films show a polarization which is up to 60% smaller than that of pure BiFeO₃ films^{24,27}. Further, first-principles calculations have predicted that substitution of Bi by La cations reduces the energy barrier between polar states by up to 50% for 25% doping. This, in turn, leads to a reduction of coercive voltages (down to 0.8 V for a 100 nm film), enabling low-power switching²⁴. Additionally, a significant reduction of switching times has been demonstrated for La_{0.15}Bi_{0.75}FeO₃ films compared to pure BiFeO₃ in a wide range of applied electric fields²⁸. Nevertheless, further improvement requires understanding the origin of the two-step polarization switching in BiFeO₃ and related materials, as well as search for other strategies for manipulating the switching energy landscape. For that purpose, dynamical simulations of polar-

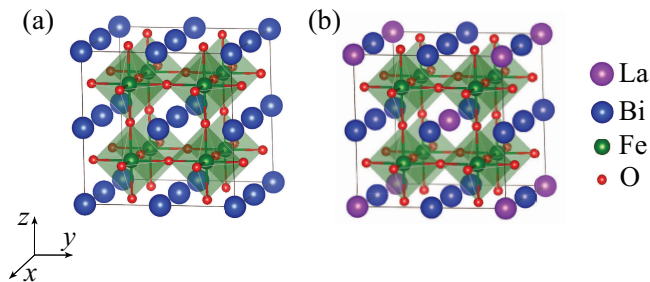


Figure 1. Sketch of the 40-atom supercell used in our simulations of (a) BiFeO_3 and (b) $\text{La}_{0.25}\text{Bi}_{0.75}\text{FeO}_3$.

ization switching based on phenomenological models of the free energy can be very helpful.

Landau free-energy potentials^{29–32}, together with the Landau-Khalatnikov time-evolution equation³³, offer a practical scheme to investigate switching in ferroelectrics. In this approach, one expands the energy of the compound around the reference paraelectric phase in powers of the relevant order parameters, keeping only terms compatible with the crystal symmetry³⁴. It is important to note that the reliability of such simulations depends on the choice of the free energy expansion's coefficients, which can be obtained either by fitting to experimental data or from first-principles calculations³⁴. In compounds as complex as BiFeO_3 , which feature multiple primary order parameters, deriving a suitable Landau potential from experimental information is all but impossible; hence, there is a clear need for the development of first-principles approaches.

In this work we introduce the simplest, lowest-order Landau-like potential able to reproduce the energies and structures of the low-energy polymorphs of BiFeO_3 and related materials. We present an analytical approach to compute the model parameters from density functional theory (DFT) and apply it to BiFeO_3 and $\text{La}_{0.25}\text{Bi}_{0.75}\text{FeO}_3$. We demonstrate the overall accuracy of the obtained potentials, and discuss an effective way to treat intermediate compositions. Finally, we discuss the physics captured by the model, namely, the interaction between polarization and FeO_6 octahedral tilts, how it affects the energetics of different BiFeO_3 polymorphs, as well as the effects of La doping.

II. COMPUTATIONAL DETAILS

All calculations are performed using the DFT^{35,36} implementation in the Vienna *Ab initio* Simulation package (VASP)³⁷. For the exchange-correlation potential, we use the generalized gradient approximation optimized for solids³⁸, with a Hubbard U correction (within Dudarev's scheme³⁹ and $U = 4$ eV) for a better treatment of iron's $3d$ electrons. We treat the interaction between core and valence electrons by the projector-augmented plane wave method^{37,40}, solving explicitly for 15 electrons of Bi

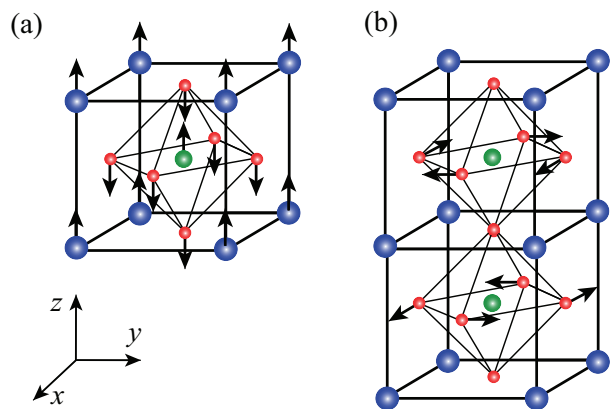


Figure 2. Ionic displacement patterns corresponding to (a) a polar distortion mode along the $[001]$ pseudocubic direction and (b) FeO_6 octahedral rotations about the same axis. Arrows indicate the directions of the ionic displacements and do not reflect their relative amplitudes. Blue, green and red circles indicate Bi, Fe and O ions, respectively.

($5d^{10}6s^26p^3$), 9 of La ($5p^66s^25d^1$), 14 of Fe ($3p^63d^74s^1$), and 6 of O ($2s^22p^4$). We use a plane-wave basis set with a cutoff energy of 500 eV. We use a $3 \times 3 \times 3$ Γ -centered Monkhorst-Pack k -point grid for reciprocal space integrals in the Brillouin zone corresponding to a 40-atom cell that is a $2 \times 2 \times 2$ multiple of the 5-atom perovskite unit (see Fig. 1(a)). We ensure that these choices provide a good level of convergence for the quantities of interest. All simulations are performed with the G-type antiferromagnetic order of Fe magnetic moments imposed. In the lattice optimizations, the structures are considered to be relaxed when the forces acting on the atoms are below 0.01 eV/Å. We calculate elastic constants by finite differences using the strain-stress relationship⁴¹.

III. FORMALISM

A. Landau-like potential

In this section we introduce the potential for BiFeO_3 and La-doped BiFeO_3 as an expansion around the reference paraelectric cubic phase in powers of the following order parameters: (i) the three-dimensional electric polarization $\mathbf{P} = (P_x, P_y, P_z)$; (ii) the antiphase rotations of FeO_6 octahedra $\mathbf{R} = (R_x, R_y, R_z)$; (iii) the strain $\boldsymbol{\eta} = (\eta_{xx}, \eta_{yy}, \eta_{zz}, \eta_{yz}, \eta_{xz}, \eta_{xy})$, where $\eta_{xx} = \epsilon_{xx}$, $\eta_{yy} = \epsilon_{yy}$, $\eta_{zz} = \epsilon_{zz}$, $\eta_{yz} = 2\epsilon_{yz}$, $\eta_{xz} = 2\epsilon_{xz}$ and $\eta_{xy} = 2\epsilon_{xy}$, and ϵ_{ij} are the components of the homogeneous strain tensor. The resulting expression for the potential (per perovskite unit cell) is written as follows:

$$F(P, R, \eta) = F_0 + F(P) + F(R) + F(\eta) + F(P, R) + F(P, \eta) + F(R, \eta). \quad (1)$$

Here, F_0 is the free energy of the reference cubic phase. $F(P)$, $F(R)$ and $F(\eta)$ are the energy contributions solely due to polarization, FeO_6 octahedral rotations and strain, respectively, which we write as follows:

$$F(P) = A_P(P_x^2 + P_y^2 + P_z^2) + B_P(P_x^2 + P_y^2 + P_z^2)^2 + C_P(P_x^2 P_y^2 + P_y^2 P_z^2 + P_z^2 P_x^2); \quad (2)$$

$$F(R) = A_R(R_x^2 + R_y^2 + R_z^2) + B_R(R_x^2 + R_y^2 + R_z^2)^2 + C_R(R_x^2 R_y^2 + R_y^2 R_z^2 + R_z^2 R_x^2); \quad (3)$$

$$F(\eta) = \frac{1}{2}C_{11}(\eta_{xx}^2 + \eta_{yy}^2 + \eta_{zz}^2) + C_{12}(\eta_{xx}\eta_{yy} + \eta_{yy}\eta_{zz} + \eta_{zz}\eta_{xx}) + \frac{1}{2}C_{44}(\eta_{yz}^2 + \eta_{xz}^2 + \eta_{xy}^2). \quad (4)$$

We truncate the expansion in \mathbf{P} and \mathbf{R} at the fourth order, which is the minimum required to model structural instabilities. In turn, we only consider harmonic terms for the strains.

Then, $F(P, R)$, $F(P, \eta)$ and $F(R, \eta)$ are the coupling terms, which we write as:

$$F(P, R) = B_{PR}(P_x^2 + P_y^2 + P_z^2)(R_x^2 + R_y^2 + R_z^2) + C_{PR}(P_x^2 R_x^2 + P_y^2 R_y^2 + P_z^2 R_z^2) + C'_{PR}(P_x P_y R_x R_y + P_y P_z R_y R_z + P_z P_x R_z R_x); \quad (5)$$

$$F(P, \eta) = \gamma_{P111}(\eta_{xx}P_x^2 + \eta_{yy}P_y^2 + \eta_{zz}P_z^2) + \gamma_{P122}(\eta_{xx}(P_y^2 + P_z^2) + \eta_{yy}(P_z^2 + P_x^2) + \eta_{zz}(P_x^2 + P_y^2)) + \gamma_{P423}(\eta_{yz}P_y P_z + \eta_{xz}P_z P_x + \eta_{xy}P_x P_y); \quad (6)$$

$$F(R, \eta) = \gamma_{R111}(\eta_{xx}R_x^2 + \eta_{yy}R_y^2 + \eta_{zz}R_z^2) + \gamma_{R122}(\eta_{xx}(R_y^2 + R_z^2) + \eta_{yy}(R_z^2 + R_x^2) + \eta_{zz}(R_x^2 + R_y^2)) + \gamma_{R423}(\eta_{yz}R_y R_z + \eta_{xz}R_z R_x + \eta_{xy}R_x R_y). \quad (7)$$

Here we restrict ourselves to the lowest-order symmetry-allowed couplings between the considered order parameters. Note that, in these equations, A , B , C , C' and γ are the material-dependent expansion coefficients that we compute using DFT as detailed in Sec. III B. The coefficients C_{11} , C_{12} , and C_{44} in Eq. (4), as well as γ parameters in Eqs. (5)-(7) are given in Voigt notation for compactness.

B. Computing the potential parameters

We now describe the approach to compute the expansion coefficients of the Landau-like potential introduced in Sec. III A. We mainly focus on an analytical approach, but also discuss briefly a numerical scheme for compari-

son.

1. Training set

We first identify the states or polymorphs that we want our models to describe. We consider the ground state as well as the low-energy polymorphs of the material, including the states that might be relevant for polarization switching. We thus define a training set of first-principles results corresponding to the energies and structures of such polymorphs.

Before we continue, let us introduce a convenient notation for the polymorphs we consider: we write “P(R)[...]c” or “P[...]R[...]c”, where the first letter, P or R, indicates whether the structure presents a polar distortion or FeO_6 octahedral tilts, respectively (if both distortions appear, we indicate it by P+R); then, [001] or [111] shows the axis along/about which the corresponding distortion is oriented; finally, “c” indicates that the cubic cell is kept fixed. Thus, for example, the polymorph P[001]c is characterized by a polar distortion along the [001] direction and its cell is fixed to that of cubic reference structure. For simplicity, we also introduce short notations for all the polymorphs of interest, such as “1c” for the state P[001]c. We summarize all the notations for the polymorphs and the corresponding order parameters in Table I.

BiFeO₃ The starting point for constructing the training set is the already-mentioned 40-atom supercell compatible with the G-type antiferromagnetic order and the antiphase rotations of the FeO_6 octahedra. First, we run a DFT simulation to optimize the volume of the cubic phase of BiFeO_3 using this supercell. Next, we use the optimized structure to construct six polymorphs (1c to 6c in Table I) by imposing the polar distortion and/or antiphase octahedral rotation along/about either the [001] or [111] directions while keeping the volume and shape of the supercell fixed (the corresponding ionic displacement patterns are illustrated in Fig. 2). We use DFT to optimize the ionic positions in these polymorphs and calculate the energies E_s of the resulting structures, where the index s labels polymorphs in the training set. Additionally, we also consider the state we call P[111]+R[111]c (7c); here, we impose a polar distortion and octahedral tilts with amplitudes typical of BiFeO_3 , but oblique to each other. This structure does not correspond to a special point of the energy landscape; therefore, we do not perform a structural optimization and only compute its energy, which is needed to obtain the coefficient C'_{PR} , as we will show in Sec. III B 2.

Next, we consider the first six polymorphs mentioned above (structures 1 to 6 in Table I), but now allowing for changes in the shape and volume of the supercell (note we omit the “c” in the notation).

In all cases we extract the displacements $\mathbf{u}_{Bi,s}$ ($u_{Bi,s}$ are in Angstrom) of the Bi cations with respect to the corresponding O anion cages. We average the values of these

Table I. Polymorphs (labeled by s) included in the training set for computing the potential's coefficients and the notations for their polarizations \mathbf{P}_s , FeO₆ octahedral rotations \mathbf{R}_s and components of the strain tensor $\boldsymbol{\eta}_s$.

	Polymorph	\mathbf{P}	\mathbf{R}	$\boldsymbol{\eta}$
1c	P[001]c	(0,0, P_{1c})	(0,0,0)	(0,0,0,0,0,0)
2c	P[111]c	(P_{2c}, P_{2c}, P_{2c})	(0,0,0)	(0,0,0,0,0,0)
3c	R[001]c	(0,0,0)	(0,0, R_{3c})	(0,0,0,0,0,0)
4c	R[111]c	(0,0,0)	(R_{4c}, R_{4c}, R_{4c})	(0,0,0,0,0,0)
5c	P[001]+R[001]c	(0,0, P_{5c})	(0,0, R_{5c})	(0,0,0,0,0,0)
6c	P[111]+R[111]c	(P_{6c}, P_{6c}, P_{6c})	(R_{6c}, R_{6c}, R_{6c})	(0,0,0,0,0,0)
7c	P[11 $\bar{1}$]+R[111]c	($P_{7c,\perp}, P_{7c,\perp}, P_{7c,\parallel}$)	($R_{7c,\perp}, R_{7c,\perp}, R_{7c,\parallel}$)	(0,0,0,0,0,0)
1	P[001]	(0,0, P_1)	(0,0,0)	($\eta_{1,\perp}, \eta_{1,\perp}, \eta_{1,\parallel}, 0, 0, 0$)
2	P[111]	(P_2, P_2, P_2)	(0,0,0)	($\eta_2, \eta_2, \eta_2, s_2, s_2, s_2$)
3	R[001]	(0,0,0)	($R_3, 0, 0$)	($\eta_{3,\parallel}, \eta_{3,\perp}, \eta_{3,\perp}, 0, 0, 0$)
4	R[111]	(0,0,0)	(R_4, R_4, R_4)	($\eta_4, \eta_4, \eta_4, s_4, s_4, s_4$)
5	P[001]+R[001]	(0,0, P_5)	(0,0, R_5)	($\eta_{5,\perp}, \eta_{5,\perp}, \eta_{5,\parallel}, 0, 0, 0$)
6	P[111]+R[111]	(P_6, P_6, P_6)	(R_6, R_6, R_6)	($\eta_6, \eta_6, \eta_6, s_6, s_6, s_6$)

displacements over all Bi ions to obtain $\bar{\mathbf{u}}_{Bi,s}$. Since the Bi off-centering largely determines the electric polarization in BiFeO₃, we estimate \mathbf{P}_s for the considered polymorphs as $\mathbf{P}_s = K_0 \bar{\mathbf{u}}_{Bi,s}$, where $K_0 = P_0 / \bar{u}_{Bi,6}$, $P_0 = 0.58$ C/m² and $\bar{\mathbf{u}}_{Bi,6}$ is the average Bi off-centering in the ground state P[111]+R[111]. This choice of P_0 ensures that the spontaneous polarization of the P[111]+R[111] polymorph is $\mathbf{P}_6 = P_0(1, 1, 1)$ which gives the magnitude of \mathbf{P}_6 around its experimentally determined value of 1 C/m².

Similarly, we compute the rotation angles of the FeO₆ octahedra \mathbf{R}_s about the pseudocubic axes, from which we obtain the amplitude of the antiphase tilt pattern, $\bar{\mathbf{R}}_s$. Finally, in the cases where the shape and volume of the cell are allowed to relax, we extract also the components of the strain tensor $\boldsymbol{\eta}_s$. The obtained results constitute our training set, which is presented in Table S1 of the Supplementary Material.

La-doped BiFeO₃ Experimentally, La dopants distribute quasi-randomly in the BiFeO₃ lattice, so that the macroscopic symmetry (cubic for the paraelectric phase, rhombohedral for the ground state) is only recovered when a sufficiently large sample volume is considered. Unfortunately, reproducing such a situation in a DFT calculation has a prohibitive computational cost; thus, here we assume that a particular highly-ordered La arrangement, where the dopants are as separated as possible from one another *and* which respects the cubic symmetry of the reference lattice, is a good approximation to the average experimental configuration. (For a 25 % La doping, the symmetric arrangement we use is shown in Fig. 1(b).) This approach allows us to derive Landau potentials for doped materials, with the experimentally relevant symmetry properties, from relatively inexpensive DFT calculations. Admittedly, a careful (computation-

ally costly) validation of its accuracy remains for future work.

Having chosen a suitable, symmetric dopant arrangement, we optimize the cubic cell of the reference paraelectric structure using DFT. Next, we use this structure to construct the sets of polymorphs 1c to 7c and 1 to 6, in analogy to the case of pure BiFeO₃. For the case of a 25 % La composition, the obtained values of \mathbf{P}_s , \mathbf{R}_s , $\boldsymbol{\eta}_s$ and E_s of their optimized structures are summarized in Table S2 of the Supplementary Material.

Note that we encountered difficulties in constructing the training set for La_{1-x}Bi_xFeO₃ compositions with an intermediate content of La ($0 < x < 0.25$). For example, for La_{0.125}Bi_{0.875}FeO₃, one can easily construct a paraelectric reference by substituting a single Bi atom in the supercell of Fig. 1(a). However, we observed that the P[001]+R[001]c and P[001]+R[001] polymorphs relax to the lower symmetry phases displaying additional (and large) in-phase rotations of the FeO₆ octahedra. These extra distortions are secondary modes activated by the symmetry breaking associated to the combination of polar and antiphase orders together with the considered arrangement of La dopants. These distortions are not expected to occur experimentally, as the La dopants are largely disordered in real samples, and such in-phase tilts may occur locally at most. Moreover, they cannot be treated within our simple potentials (an explicit consideration of in-phase tilts would be required) and complicate the definition of the training set. Hence, here we do not compute models for such intermediate compositions. Nevertheless, as we show in Sec. IV C, suitable potentials can be obtained by interpolation between those obtained for neighboring (well-behaved) compositions.

Table II. Conditions used to derive the analytical expressions for the potential's coefficients. $E_s|\phi_{s,eq}$ denotes the energy of the polymorph s corresponding to the equilibrium value of order parameter ϕ_s . $\lambda = 1 \text{ m}^4 \text{ deg}^2 / \text{C}^2$ is an *ad hoc* coefficient used to balance the units for the terms in f_{5c} and f_{6c} (see text).

Conditions	
A_P	
B_P	$\frac{\partial E_{1c}}{\partial P_{1c}} = 0; \frac{\partial E_{2c}}{\partial P_{2c}} = 0; E_{1c} _{P_{1c,eq}}; E_{2c} _{P_{2c,eq}}$
C_P	
A_R	
B_R	$\frac{\partial E_{3c}}{\partial R_{3c}} = 0; \frac{\partial E_{4c}}{\partial R_{4c}} = 0; E_{3c} _{R_{3c,eq}}; E_{4c} _{R_{4c,eq}}$
C_R	
B_{PR}	
C_{PR}	$\frac{\partial E_{5c}}{\partial P_{5c}} + \lambda \frac{\partial E_{5c}}{\partial R_{5c}} = 0; \frac{\partial E_{6c}}{\partial P_{6c}} + \lambda \frac{\partial E_{6c}}{\partial R_{6c}} = 0; E_{7c}$
C'_{PR}	
γ_{P111}	$\frac{\partial E_6}{\partial \eta_6} = 0$
γ_{P122}	$\frac{\partial E_1}{\partial \eta_{1,\perp}} = 0; \frac{\partial E_2}{\partial \eta_2} = 0$
γ_{P423}	$\frac{\partial E_6}{\partial s_6} = 0$
γ_{R111}	$\frac{\partial E_3}{\partial \eta_{3,\perp}} = 0$
γ_{R122}	$\frac{\partial E_3}{\partial \eta_{3,\perp}} = 0; \frac{\partial E_4}{\partial \eta_4} = 0$
γ_{R423}	$\frac{\partial E_4}{\partial s_4} = 0$

2. Analytical approach

The approach introduced in this section allows full control of the information used to compute the parameters of the potential. To achieve that, we derive an analytical expression for each of the potential coefficients, in terms of E_s , \mathbf{P}_s , \mathbf{R}_s and $\boldsymbol{\eta}_s$ of the polymorphs in the training set (see Sec. III B 1). To obtain such formulas, we use Eqs. (1) - (7) and impose the zero-derivative condition $\partial F / \partial \phi_{i,s} = 0$, where $\phi_{i,s}$ is the i th component of order parameter ϕ evaluated for polymorph s . Let us illustrate our procedure by presenting in detail the case of the parameters A_P , B_P and C_P of Eq. 2.

We consider two polar-only polymorphs with fixed cubic cell, P[001]c (1c) and P[111]c (2c), and use the notation for their polarization components introduced in Table I, $\mathbf{P}_{1c} = (0, 0, P_{1c})$ and $\mathbf{P}_{2c} = (P_{2c}, P_{2c}, P_{2c})$. Then, from Eq. (2) we can write the polymorph energies

$$E_{1c} = A_P P_{1c}^2 + B_P P_{1c}^4 \quad (8)$$

and

$$E_{2c} = 3A_P P_{2c}^2 + 3(3B_P + C_P) P_{2c}^4. \quad (9)$$

By taking the derivatives of these energies with respect to P_{1c} and P_{2c} , and setting them equal to zero, we obtain the following equations for the equilibrium values of P_{1c} and P_{2c} :

$$P_{1c}^2 = -\frac{A_P}{2B_P} \quad (10)$$

and

$$P_{2c}^2 = -\frac{A_P}{2(3B_P + C_P)}. \quad (11)$$

Then, by using these expressions in Eqs. (8) and (9), we obtain, respectively, E_{1c} and E_{2c} as functions of the parameters of the potential, such as

$$E_{1c} = -\frac{A_P^2}{4B_P} \quad (12)$$

and

$$E_{2c} = -\frac{3A_P^2}{4(3B_P + C_P)}. \quad (13)$$

From Eq. (11) one can see that $3B_P + C_P = -A_P/2P_{2c}^2$. By using this in Eq. (13), one can straightforwardly obtain the analytical expression for A_P :

$$A_P = \frac{2E_{2c}}{3P_{2c}^2}. \quad (14)$$

From Eq. (12), in turn, one can obtain:

$$B_P = -\frac{A_P^2}{4E_{1c}}. \quad (15)$$

Finally, by combining Eqs. (13), (14) and (15), we get:

$$C_P = \frac{3A_P^2}{4} \left(\frac{1}{E_{1c}} - \frac{1}{E_{2c}} \right). \quad (16)$$

Since E_{1c} , E_{2c} , P_{1c} and P_{2c} are known from our first-principles calculations described above, the coefficients A_P , B_P and C_P can be directly computed using Eqs. (14), (15) and (16), respectively.

Similarly, we can derive the analytical expressions for the remaining coefficients of our potential. The specific conditions and properties used in the derivation are summarized in Table II, and the resulting expressions are:

$$A_R = \frac{2E_{4c}}{3R_{4c}^2}; \quad (17)$$

$$B_R = \frac{-A_R^2}{4E_{3c}}; \quad (18)$$

$$C_R = \frac{3A_R^2}{4} \left(\frac{1}{E_{3c}} - \frac{1}{E_{4c}} \right); \quad (19)$$

$$B_{PR} = \frac{f_{7c} - f_{5c}(C_{7c} - C'_{7c}) - \frac{1}{3}C'_{7c}f_{6c}}{B_{7c} - C_{7c} - 2C'_{7c}}, \quad (20)$$

where

$$B_{7c} = (2P_{7c,\perp}^2 + P_{7c,\parallel}^2)(2R_{7c,\perp}^2 + R_{7c,\parallel}^2), \quad (21)$$

$$C_{7c} = 2P_{7c,\perp}^2 R_{7c,\perp}^2 + P_{7c,\parallel}^2 R_{7c,\parallel}^2, \quad (22)$$

$$C'_{7c} = P_{7c,\perp}^2 R_{7c,\perp}^2 + 2P_{7c,\perp} P_{7c,\parallel} R_{7c,\perp} R_{7c,\parallel}, \quad (23)$$

$$f_{5c} = -\frac{A_P + \lambda A_R + 2B_P P_{5c}^2 + 2\lambda B_R R_{5c}^2}{\lambda P_{5c}^2 + R_{5c}^2} \quad (24)$$

and

$$f_{6c} = -\frac{1}{\lambda P_{6c}^2 + R_{6c}^2} (3A_P + 3\lambda A_R + 6(3B_P + C_P)P_{6c}^2 + 6\lambda(3B_R + C_R)R_{6c}^2), \quad (25)$$

where $\lambda = 1 \text{ m}^4 \text{ deg}^2 / \text{C}^2$ is an *ad hoc* coefficient that allows us to combine two zero-derivative conditions (for polarization and tilts, respectively) into only one. Further, we have

$$f_{7c} = E_{7c} - (A_P(2P_{7c,\perp}^2 + P_{7c,\parallel}^2) + B_P(2P_{7c,\perp}^2 + P_{7c,\parallel}^2)^2 + C_P(P_{7c,\perp}^4 + 2P_{7c,\perp}^2 P_{7c,\parallel}^2) + A_R(2R_{7c,\perp}^2 + R_{7c,\parallel}^2) + B_R(2R_{7c,\perp}^2 + R_{7c,\parallel}^2)^2 + C_R(R_{7c,\perp}^4 + 2R_{7c,\perp}^2 R_{7c,\parallel}^2)); \quad (26)$$

$$C_{PR} = f_{5c} - B_{PR}; \quad (27)$$

$$C'_{PR} = \frac{1}{C'_{7c}} (f_{7c} - B_{7c}B_{PR} - C_{7c}C_{PR}); \quad (28)$$

$$\gamma_{P122} = \frac{(C_{12} - C_{11})\eta_{1,\perp}}{P_1^2} - \frac{C_{12}\eta_2}{P_2^2}; \quad (29)$$

$$\gamma_{P111} = -2\gamma_{P122} - \left(\eta_6 + \frac{(\gamma_{R111} + 2\gamma_{R122})R_6^2}{C_{11} + 2C_{12}} \right) \frac{C_{11} + 2C_{12}}{P_6^2}; \quad (30)$$

$$\gamma_{P423} = - \left(s_6 + \frac{\gamma_{R423}R_6^2}{C_{44}} \right) \frac{C_{44}}{P_6^2}; \quad (31)$$

$$\gamma_{R111} = \frac{2(C_{11} - C_{12})\eta_{3,\perp}}{R_3^2} - \frac{C_{11}\eta_4}{R_4^2}; \quad (32)$$

$$\gamma_{R122} = \frac{(C_{12} - C_{11})\eta_{3,\perp}}{R_3^2} - \frac{C_{12}\eta_4}{R_4^2}; \quad (33)$$

and

$$\gamma_{R423} = -\frac{C_{44}s_4}{R_4^2}. \quad (34)$$

Note, that it is possible to choose other conditions, different from those in Table II, to derive the expressions for the model parameters. For example, γ_{P111} might be obtained from the energies and structures of polar-only polymorphs, in analogy to what we do for γ_{R111} using tilt-only polymorphs. However, we find that this choice yields shear strains with incorrect sign for the P[111]+R[111] ground state of BiFeO₃. By contrast, the condition we use to compute γ_{P111} (i.e., $\partial E_6 / \partial \eta_6 = 0$) includes the information about the ground state and corrects this problem. These difficulties reflect the simplicity of our low-order polynomial model, which can account (exactly) for only a small number of properties.

Finally, the elastic constants C_{11} , C_{12} and C_{44} are calculated directly from DFT.

3. Numerical approach

The numerical approach that we introduce in this section allows to compute the potential coefficients using the information from all considered structural polymorphs. We focus here on the case of pure BiFeO₃, noting that exactly the same procedure can be applied to La_{0.25}Bi_{0.75}FeO₃.

We work with the BiFeO₃ polymorphs from the training set introduced in Sec. III B 1, namely, 1c to 7c and 1 to 6 of Table I. Based on the energies (E_s) and structural parameters (\mathbf{P}_s , \mathbf{R}_s , and $\boldsymbol{\eta}_s$) obtained from DFT, we construct an overdetermined system of linear equations, with the potential parameters as unknowns, using the expressions for the energy and zero derivatives corresponding to all polymorphs. (For the 7c state, the zero-derivative condition does not apply. Also, we use the elastic constants C_{11} , C_{12} and C_{44} directly obtained from DFT.)

We find that the potential obtained using this approach provides less accurate predictions for the properties of the low-energy polymorphs of BiFeO₃ as compared to the analytical approach introduced in Sec. III B 2 (see details in Sec. SII of the Supplementary material). More specifically, the numerically-determined potential does a better job at reproducing some features (e.g., the polarization of the P[001] state) that we disregard in our analytical approach. In turn, it is less accurate when it comes to capture some critical properties (e.g., the ground state energy). We conclude that, while this fitting approach

Table III. Coefficients of our Landau-like potentials calculated for BiFeO₃ (BFO) and La_{0.25}Fe_{0.75}FeO₃ (LBFO) using the analytical approach introduced in Sec. III B 2. We give energies per 5-atom perovskite unit cell.

	BFO	LBFO	Units
A_P	-1.747	-1.674	$\times 10^{-19}$, J m ⁴ C ⁻²
B_P	1.070	1.286	$\times 10^{-19}$, J m ⁸ C ⁻⁴
C_P	-7.486	-6.212	$\times 10^{-20}$, J m ⁸ C ⁻⁴
A_R	-8.555	-7.560	$\times 10^{-22}$, J deg ⁻²
B_R	2.169	1.962	$\times 10^{-24}$, J deg ⁻⁴
C_R	-1.240	-0.848	$\times 10^{-24}$, J deg ⁻⁴
C_{11}	1.833	1.754	$\times 10^{-17}$, J
C_{12}	7.301	11.280	$\times 10^{-18}$, J
C_{44}	4.600	4.262	$\times 10^{-18}$, J
B_{PR}	1.121	1.183	$\times 10^{-21}$, J m ⁴ C ⁻² deg ⁻²
C_{PR}	-3.437	-3.319	$\times 10^{-22}$, J m ⁴ C ⁻² deg ⁻²
C'_{PR}	-2.245	-2.219	$\times 10^{-21}$, J m ⁴ C ⁻² deg ⁻²
γ_{P111}	-9.444	-7.866	$\times 10^{-19}$, J m ⁴ C ⁻²
γ_{P122}	-1.557	-4.898	$\times 10^{-19}$, J m ⁴ C ⁻²
γ_{P423}	-3.232	-3.359	$\times 10^{-19}$, J m ⁴ C ⁻²
γ_{R111}	-1.178	0.482	$\times 10^{-21}$, J deg ⁻²
γ_{R122}	1.158	-10.026	$\times 10^{-22}$, J deg ⁻²
γ_{R423}	1.155	1.022	$\times 10^{-21}$, J deg ⁻²

might work well for more complete, higher-order potentials (for example, such as the one introduced in Ref. 42), it seems less suitable for computing the parameters of our low-order model. Therefore, in the following, we are going to discuss only the results obtained using the analytical approach.

IV. RESULTS

A. BiFeO₃

In this section, we analyze how accurately the potential introduced in Sec. III A predicts the properties of BiFeO₃ polymorphs. We begin by computing the coefficients of the potential following the analytical approach described in Sec. III B 2. The resulting values are presented in Table III. Next, we use the computed potential to calculate the equilibrium properties (\mathbf{P}_s , \mathbf{R}_s , $\boldsymbol{\eta}_s$, and E_s) of the polymorphs 1c to 6c and 1 to 6. Since in these polymorphs the form of \mathbf{P}_s is either (0, 0, P_s) or (P_s , P_s , P_s) (the same holds for \mathbf{R}_s), in the following we will discuss single components of \mathbf{P}_s and \mathbf{R}_s (P_s and R_s , respectively). We plot the values of P_s , R_s and E_s predicted using our potential versus their DFT counterparts as shown in Fig. 3 (all these values, as well as the components of $\boldsymbol{\eta}_s$ are also presented in Table S1 of the Supplementary Material). We note that, if the model prediction and DFT value match exactly, the corresponding point lays on the black dashed line.

First, we discuss the BiFeO₃ polymorphs with the fixed cubic cell (no strain relaxation). From Figs. 3(a) and

3(b) one can see that, for these polymorphs, our model predicts P_s and R_s in nearly perfect agreement with DFT. As shown in Fig. 3(c), it also reproduces accurately their energies and, therefore, their relative stability. Indeed, among the structures having only polar distortion (P[001]c and P[111]c), the one with $\mathbf{P} \parallel [111]$ is lower in energy according to both model and DFT. The same holds for the structures having only FeO₆ octahedral rotations (R[111]c is lower in energy than R[001]c). Overall, the lowest energy structure is P[111]+R[111]c, in which both distortions coexist and oriented along/about [111]. Here, one should keep in mind that DFT information about these polymorphs is explicitly used to compute the model parameters (see Table II), hence the agreement is not surprising. Nevertheless, the potential does provide accurate predictions for quantities that are not considered in its derivation (e.g., P of P[001]c, R of R[001]c, and E_s of P[001]+R[001]c and P[111]+R[111]c).

Next, we consider the BiFeO₃ polymorphs with allowed strain relaxation (Figs. 3(d)-(f)). In this case, our potential also provides accurate predictions for all considered quantities for the most of the considered polymorphs; in particular, it yields the correct ground state of BiFeO₃ (P[111]+R[111]). There is only one polymorph for which the model is less accurate, namely, P[001]. In this case, the DFT optimized structure has a large distortion along the z axis (the c/a ratio is approximately 1.27), accompanied by a large P_z ; this is usually called supertetragonal phase^{43,44}. This behavior is not well captured by our potential, as it underestimates the polarization and strains components compared to the DFT values ($P_z = 1.039$ versus 1.624 C/m²; $\eta_{xx} = -0.012$ versus -0.044 ; $\eta_{zz} = 0.065$ versus 0.216). This issue is also reflected in the energy predicted for this phase. From the DFT results one can see that, among the polymorphs with only polar distortion, the strain relaxation stabilizes the supertetragonal phase over the rhombohedral one (P[001] is lower than P[111] by 0.023 eV/f.u). Our model does predict the energy lowering of P[001] state due to the strain relaxation (the negative γ_{P111} coupling results in large P_z and η_{zz}). However, since it underestimates P_z and η_{zz} , this energy reduction is not enough to stabilize P[001] over P[111]. Note that these deficiencies were to be expected, as we decided to use a minimal amount of DFT information on the supertetragonal phase when deriving the parameters of our model (see Table II), because this state is not relevant for our ultimate purpose of studying polarization switching in the rhombohedral phase of BiFeO₃. Moreover, we checked that, if we try to capture the supertetragonal c/a , this makes it difficult to obtain a correct prediction for the ground state, as the P[001] state tends to become dominant.

B. La_{0.25}Bi_{0.75}FeO₃

Now we discuss the case of La_{0.25}Bi_{0.75}FeO₃. We first compute the parameters of the potential using the ana-

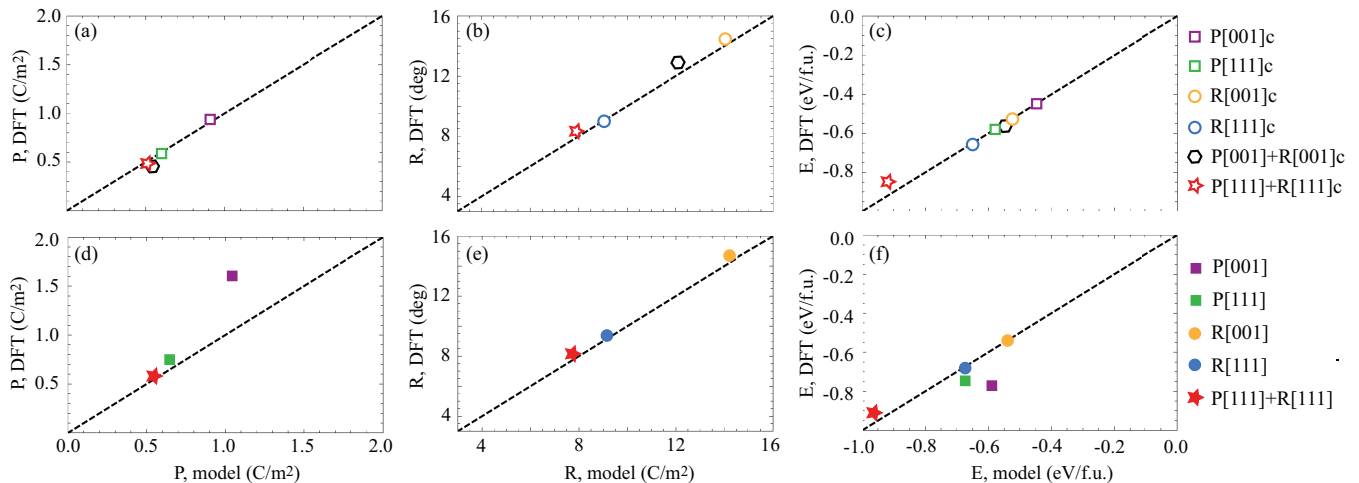


Figure 3. Structural properties and energies of BiFeO₃ polymorphs predicted using the Landau-like potential and plotted versus their corresponding DFT values. The top row shows the results obtained for the polymorphs with fixed cubic supercell (no strain), while the bottom row shows the properties of the polymorphs with fully relaxed cells. Panels (a) and (d) show the electric polarization P , (b) and (e) the FeO₆ octahedral rotations R , (c) and (f) the energies E . The polymorph P[001]+R[001] is not shown in panels (d) - (f), since its fully relaxed structure has very small FeO₆ octahedral rotations ($R = 0.066^\circ$) and our model predicts it to be zero, therefore reducing to the state P[001].

lytical expressions in Sec. III B 2. The resulting values are presented in Table III. Next, we compare the model predictions and DFT values for our considered polymorphs in Fig. 4 (these results are also summarized in Table S2 of the Supplementary Material, together with the corresponding strains).

Let us first consider the polymorphs with fixed cubic cell (Fig. 4(a)-(c)). Our potential provides very accurate predictions for polarizations and tilts, similarly to the case of pure BiFeO₃. The energy and relative stability of these polymorphs is also well captured by the model. Indeed, for polar-only structures both the model and DFT predict the rhombohedral P[111]c state to be lower in energy than the tetragonal P[001]c phase. The same holds for the polymorphs having only FeO₆ rotations: R[111]c is lower in energy than R[001]c. Note that the energy difference between the structures with tetragonal and rhombohedral phases are reduced compared to the case of pure BiFeO₃. The lowest-energy phase is P[111]+R[111]c, where polarization and tilts co-exist.

For the polymorphs in which shape and volume of the cell are allowed to relax, we observe the following. First, the model predicts accurate values of the polarization in all cases except for P[001]. Indeed, for the supertetragonal state, the predicted P_s and η_{zz} are underestimated relative to the DFT values. This issue is also reflected in the energy of the polymorph: our potential predicts P[001] to be the highest-energy state, while DFT shows that this phase is the second-lowest in energy, right above the P[111]+R[111] ground state. Additionally, we find that the tilts are accurately predicted by our model for all polymorphs except R[001]; in that case, the tilt amplitude and the strains are exaggerated compared to

the DFT values. Note that, as it was the case for pure BiFeO₃, these deficiencies are the result of the limited amount of DFT information on states P[001] and R[001] that was used to derive the parameters of our model.

C. Intermediate compositions

In this section we demonstrate how our potentials can be used to study La_{1-x}Bi_xFeO₃ with intermediate La content, $0 < x < 0.25$. We focus on the case of La_{0.125}Bi_{0.875}FeO₃ and check whether the properties of the polymorphs from the training set can be predicted by linear interpolation between BiFeO₃ and La_{0.25}Bi_{0.75}FeO₃.

We consider two types of interpolation. First, we construct a model for $x = 0.125$ with coefficients obtained from interpolation of the corresponding values for the $x = 0$ and $x = 0.25$ cases. Using this model, we can easily predict the properties (P_s , R_s and E_s) of all the polymorphs in the training set. Second, we derive the very same properties by direct interpolation of the values obtained at $x = 0$ and $x = 0.25$. In Fig. 5 we compare the quantities thus obtained, and also include the corresponding DFT values for the polymorphs for which the information is available (see figure caption). We find that both interpolation approaches yield very similar predictions. Further, the agreement with DFT is good except for the supertetragonal P[001] phase, where our predictions suffer from the issues discussed above. Hence, we conclude that our models give us a way to treat compounds with intermediate compositions.

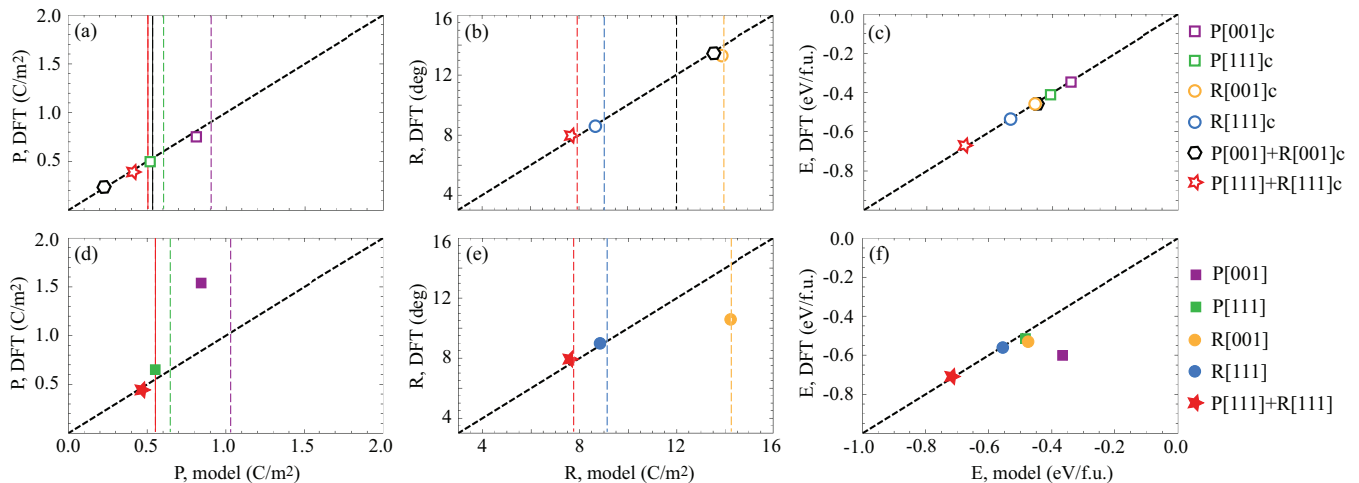


Figure 4. Structural properties and energies of $\text{La}_{0.25}\text{Bi}_{0.75}\text{FeO}_3$ polymorphs predicted using the Landau-like potential and plotted versus their corresponding DFT values. The top row shows the results obtained for the polymorphs with fixed cubic supercell (no strain), while the bottom row shows the properties of the polymorphs with fully relaxed cells. Panels (a) and (d) show the electric polarization P , (b) and (e) the FeO_6 octahedral rotations R , (c) and (f) the energies E . The polymorph $\text{P}[001]+\text{R}[001]$ is not shown in panels (d) - (f), since its fully relaxed structure has very small FeO_6 octahedral rotations ($R = 0.006^\circ$) and our model predicts it to be zero, therefore reducing to the state $\text{P}[001]$. The vertical dashed lines in panels (a), (b), (d) and (e) indicate the corresponding quantities for pure BiFeO_3 .

V. DISCUSSION

Let us now discuss the physical insights that our models provide.

A. P-R coupling

As it is well known from both experiments and computations, and correctly captured by our models, the ground state of BiFeO_3 has rhombohedral symmetry with $\mathbf{P} \parallel [111]$ and $\mathbf{R} \parallel [111]$. It is interesting to note, though, that the DFT energy of the polar-only BiFeO_3 polymorph $\text{P}[001]$ is lower than that of $\text{P}[111]$. By contrast, among the polymorphs having only FeO_6 octahedral tilts, $\text{R}[111]$ is the lowest-energy structure. These observations yield one important conclusion: that the rhombohedral symmetry of the BiFeO_3 's ground state critically depends on the presence of the octahedral tilts, as in their absence the material would be tetragonal.

In order to understand how the rhombohedral ground state of BiFeO_3 comes about, we consider the $F(P, R)$ part of our potential (Eq. 5) describing the coupling between polarization and octahedral rotations. The second term in Eq. (5), with $C_{PR} < 0$ (see Table III), favors states where \mathbf{P} and \mathbf{R} are along/about any $\langle 111 \rangle$ direction, as for example, $\mathbf{P} \parallel [111]$ and $\mathbf{R} \parallel [\bar{1}\bar{1}\bar{1}]$. In turn, the third term, with $C'_{PR} < 0$, favors phases where the FeO_6 tilts are about the axis defined by the polarization. Overall, these couplings lead \mathbf{P} and \mathbf{R} to appear together and aligned along/about the same $\langle 111 \rangle$ direction. Thus, these are the interactions driving the stabilization of the ground state phase of BiFeO_3 , rhombohedral and with

co-existing polarization and tilts.

Does this mean, however, that \mathbf{P} and \mathbf{R} cooperate in BiFeO_3 ? We address this question by considering the energy diagram presented in Fig. 6. Here we show the energies of the $\text{P}[111]\text{c}$, $\text{R}[111]\text{c}$, and $\text{P}[111]+\text{R}[111]\text{c}$ polymorphs as given by our model (E_{2c} , E_{4c} and E_{6c} , respectively, see Table IV). We also show the energy of a virtual state in which $\mathbf{P} \parallel [111]$ coexists with $\mathbf{R} \parallel [111]$ but where these order parameters are not coupled. The energy of this virtual state is simply given by $E_{2c} + E_{4c}$, taking the cubic phase as the zero of energy. Clearly, the $\text{P}[111]+\text{R}[111]\text{c}$ polymorph is higher in energy than the non-interacting virtual state and their energy difference arises from the coupling between \mathbf{P} and \mathbf{R} in $\text{P}[111]+\text{R}[111]\text{c}$ structure. To understand this, we again consider the term $F(P, R)$ (Eq. 5) with the corresponding coefficients B_{PR} , C_{PR} and C'_{PR} presented in Table III for BiFeO_3 . For the polymorph $\text{P}[111]+\text{R}[111]\text{c}$, we have $P_x = P_y = P_z = P_{6c}$ and $R_x = R_y = R_z = R_{6c}$; therefore, $F_{6c}(P, R) = 3(3B_{PR} + C_{PR} + C'_{PR})P_{6c}^2 R_{6c}^2$ for this state. In this expression, $3B_{PR} > 0$ dominates over $C_{PR} + C'_{PR} < 0$ and leads to a ground state energy that is higher than that of the virtual non-interacting state.

Thus, we find that, overall, the \mathbf{P} and \mathbf{R} order parameters compete in BiFeO_3 ($B_{PR} > 0$ dominates). Nevertheless, the polar and tilt instabilities are so strong that this repulsive interaction is not enough to prevent them from occurring simultaneously. Further, the \mathbf{P} - \mathbf{R} competition is minimized when the order parameters are oriented along/about the same $\langle 111 \rangle$ axis ($C_{PR}, C'_{PR} < 0$), which yields the rhombohedral ground state phase of BiFeO_3 .

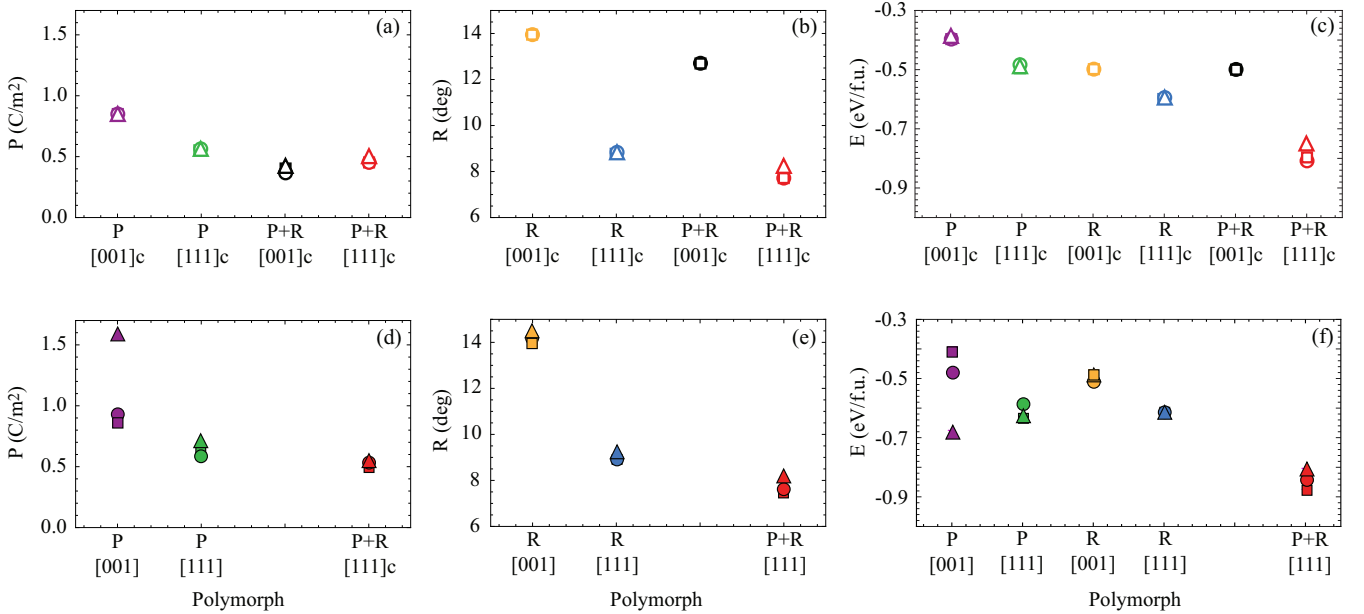


Figure 5. Structural properties and energies of $\text{La}_{0.125}\text{Bi}_{0.875}\text{FeO}_3$ polymorphs. Squares show the model predictions for P , R and E obtained using the interpolated potential’s coefficients, circles - the values obtained by direct interpolation of the corresponding results between pure BiFeO_3 and $\text{La}_{0.25}\text{Bi}_{0.75}\text{FeO}_3$, triangles - DFT values. The top row shows the results for fixed cubic cell (no strain), the bottom row - the results after a full strain relaxation. Panels (a) and (d) show the electric polarization P , (b) and (e) the FeO_6 octahedral rotations R , (c) and (f) the energies E . A missing DFT data point in the plot means that the structure of the corresponding polymorph developed non-negligible additional distortions during the DFT optimization, as described in Sec. III B 1.

B. Effects of La doping

Let us first consider how La doping affects the electric polarization. From Figs. 4(a) and 4(d) one can see that, for all considered polar polymorphs in the training set, a 25% La doping leads to reduction of P . Indeed, for the polymorphs with fixed cubic cell (Fig. 4(a)) we obtain a reduction of P by 11 – 19% for P[001]c, P[111]c and P[111]+R[111]c, and an even larger reduction for P[001]+R[001]c ($\approx 59\%$). When we allow the cell to relax (Fig. 4(d)), the obtained P reduction is in the range of 5 – 20%.

Next, let us turn to the effect of La doping on the FeO_6 octahedral tilts. As one can see from Figs. 4(b) and 4(e), the presence of 25% La has a relatively small effect (reduction) in the amplitude of tilts. More precisely, we find that the R[001]c, R[111]c and P[111]+R[111]c polymorphs with fixed cubic cell present 1 – 4% smaller R compared to pure BiFeO_3 . The exception is the P[001]+R[001]c state, where La doping leads to an increase in R by 12%. Finally, when we allow the cell to relax, we find a 0.06 – 4% reduction of R in all considered polymorphs.

Our models allow us to rationalize the most important results described above. Let us start by noting that the **P-R** couplings (B_{PR} , C_{PR} and C'_{PR} in $F(P, R)$) are not significantly affected by the doping. Hence, they do not play a significant role to explain the La-induced effects.

Table IV. Energies E_s of BiFeO_3 polymorphs calculated using DFT and predicted by the Landau-like potential introduced in this work (the coefficients of the potential are obtained using the analytical approach described in Sec. III B 2). Energy values are relative to the energy of the reference cubic phase and given in eV per 5-atom unit cell.

	Polymorph	E_s (DFT)	E_s (Model)
1c	P[001]c	-0.445	-0.445
2c	P[111]c	-0.580	-0.580
3c	R[001]c	-0.527	-0.527
4c	R[111]c	-0.651	-0.650
5c	P[001]+R[001]c	-0.556	-0.546
6c	P[111]+R[111]c	-0.853	-0.919
1	P[001]	-0.764	-0.589
2	P[111]	-0.741	-0.677
3	R[001]	-0.536	-0.540
4	R[111]	-0.679	-0.671
5	P[001]+R[001]	-0.764	-0.593
6	P[111]+R[111]	-0.909	-0.967

Indeed, the effects of La doping on the polarization are essentially captured by the changes in the $F(P)$ term of the potential (Eq. 2). As shown in Table III, we find that A_P (quadratic coupling) is reduced in magnitude upon

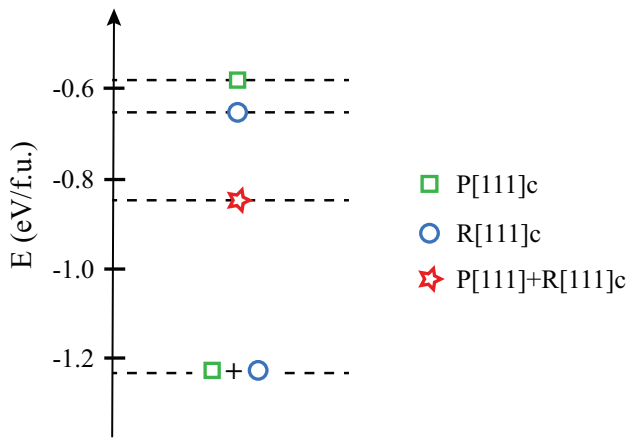


Figure 6. Model energies of several BiFeO_3 polymorphs. The lowest energy configuration corresponds to the virtual state in which $\mathbf{P} \parallel [111]$ and $\mathbf{R} \parallel [111]$ coexist but are not coupled (see text).

doping, indicating a weaker ferroelectric instability of the cubic phase. Additionally, both B_P and C_P increase and the relevant combination, $3B_P + C_P > 0$, becomes larger; hence, the quartic couplings have a stronger effect on the energy landscape compared to pure BiFeO_3 . All these changes cooperate to yield shallower ferroelectric energy wells associated to $F(P)$ for La-doped BiFeO_3 , with smaller equilibrium polarization and lower energy barrier between states of opposite \mathbf{P} . Note that this is consistent with previous studies on the effect of La-doping on the switching characteristics of BiFeO_3 ^{24,28}.

As regards the tilt energy given by $F(R)$, Table III shows that the presence of La weakens the cubic-phase instability (A_R becomes less negative); by contrast, the quartic term ($3B_R + C_R > 0$) gets reduced upon doping, thus favoring larger tilts. These changes oppose each other, and result in the generally observed moderate reduction in the amplitude of the FeO_6 rotations.

Finally, as shown in Fig. 4, the $\text{P}[001]+\text{R}[001]\text{c}$ case is peculiar, as it presents the largest reduction in P (about 59 %) and is the only one displaying an increase of R (about 12 %). We can rationalize this result by noting that, for this state, the quartic part of the energy in $F(P)$ (resp. $F(R)$) is controlled by the B_P (resp. B_R) coupling alone. Upon doping B_P grows (B_R decreases), which favors smaller polarizations (larger tilts). Further, because of the strong competition between polarization and tilts in tetragonal states ($B_{PR} > 0$; C_{PR} and C'_{PR} do not contribute), the changes get particularly large in the case of $\text{P}[001]+\text{R}[001]\text{c}$. Note also a subtle difference between $\text{P}[001]+\text{R}[001]\text{c}$ and $\text{P}[111]+\text{R}[111]\text{c}$. In the latter case, the relevant quartic parameter for the tilts is $3B_R + C_R$, and the La-induced decrease in B_R is partly

compensated by the increase in C_R ; as a result, the tilts do not grow at all (recall $A_R < 0$ grows upon doping) and the decrease of the polarization is relatively small.

Note that all these observations are consistent with what we know about the atomistic origin of the polar and tilt instabilities in BiFeO_3 . The former rely on the presence of stereochemically active $6s$ lone pairs in the Bi^{3+} cations; hence, their partial substitution by lone-pair-free La cations naturally leads to smaller polarizations. The latter are mainly controlled by the ionic radius of the Bi^{3+} cation; since La^{3+} is similar in size, the doping leaves R largely unaffected.

VI. CONCLUSIONS

In summary, we have introduced the simplest, lowest-order Landau-like potential for BiFeO_3 and related compounds, as well as methods that allow to compute the potential parameters from Density Functional Theory (DFT). More precisely, we have derived analytical expressions for all the model coefficients as functions of the energies and structural features (polarization, FeO_6 octahedral tilts and strains) of a small set of relevant polymorphs. We have applied the proposed approach to BiFeO_3 and $\text{La}_{0.25}\text{Bi}_{0.75}\text{FeO}_3$, showing its overall accuracy in reproducing the DFT data. We have also showed that our models can be used – by interpolation – to predict the properties of compounds with intermediate dopant concentrations. We note that the introduced potential, as well as the analytical scheme to obtain its coefficients from DFT, can be readily applied to study the properties of other perovskite oxides characterized by the same order parameters (polarization, antiphase oxygen-octahedral tilts, strains). This includes ferroelectrics where the tilts are not important (e.g., BaTiO_3 or PbTiO_3), antiferrodistortive non-polar perovskites (e.g., LaAlO_3), or compounds where both distortions play a relevant role (e.g., SrTiO_3), as well as their corresponding solid solutions. In principle, an extension of our scheme to compounds where other order parameters are relevant (e.g., in-phase tilts in orthorhombic perovskites like CaTiO_3 ⁴⁵) should be straightforward.

VII. ACKNOWLEDGEMENTS

We thank John M. Mangeri for the fruitful discussions. Work funded by the the Semiconductor Research Corporation and Intel via contract no. 2018-IN-2865. We also acknowledge the support of the Luxembourg National Research Fund through Grant FNR/C18/MS/12705883/REFOX/Gonzalez.

* natalya.fedorova@list.lu

† jorge.iniguez@list.lu

- ¹ N. A. Spaldin and M. Fiebig, *Science* **309**, 391 (2005).
- ² W. Eerenstein, N. D. Mathur, and J. F. Scott, *Nature* **442**, 759 (2006), ISSN 1476-4687.
- ³ G. Catalan and J. F. Scott, *Advanced Materials* **21**, 2463 (2009).
- ⁴ J. Moreau, C. Michel, R. Gerson, and W. James, *Journal of Physics and Chemistry of Solids* **32**, 1315 (1971), ISSN 0022-3697.
- ⁵ R. T. Smith, G. D. Achenbach, R. Gerson, and W. J. James, *Journal of Applied Physics* **39**, 70 (1968).
- ⁶ C. Michel, J.-M. Moreau, G. D. Achenbach, R. Gerson, and W. James, *Solid State Communications* **7**, 701 (1969), ISSN 0038-1098.
- ⁷ F. Kubel and H. Schmid, *Acta Crystallographica Section B* **46**, 698 (1990).
- ⁸ R. Seshadri and N. A. Hill, *Chemistry of Materials* **13**, 2892 (2001), ISSN 0897-4756.
- ⁹ D. Lebeugle, D. Colson, A. Forget, and M. Viret, *Applied Physics Letters* **91**, 022907 (2007).
- ¹⁰ J. Wang, J. B. Neaton, H. Zheng, V. Nagarajan, S. B. Ogale, B. Liu, D. Viehland, V. Vaithyanathan, D. G. Schlom, U. V. Waghmare, et al., *Science* **299**, 1719 (2003), ISSN 0036-8075.
- ¹¹ A. M. Glazer, *Acta Crystallographica Section B* **28**, 3384 (1972).
- ¹² C. Ederer and N. A. Spaldin, *Phys. Rev. Lett.* **95**, 257601 (2005).
- ¹³ O. Diéguez, O. E. González-Vázquez, J. C. Wojdeł, and J. Íñiguez, *Phys. Rev. B* **83**, 094105 (2011).
- ¹⁴ V. Bhide and M. Multani, *Solid State Communications* **3**, 271 (1965), ISSN 0038-1098.
- ¹⁵ I. Dzyaloshinsky, *Journal of Physics and Chemistry of Solids* **4**, 241 (1958), ISSN 0022-3697.
- ¹⁶ T. Moriya, *Phys. Rev.* **120**, 91 (1960).
- ¹⁷ I. Sosnowska, T. P. Neumaier, and E. Steichele, *Journal of Physics C: Solid State Physics* **15**, 4835 (1982).
- ¹⁸ I. Sosnowska, W. Schäfer, W. Kockelmann, K. H. Andersen, and I. O. Troyanchuk, *Applied Physics A* **74**, s1040 (2002), ISSN 1432-0630.
- ¹⁹ F. Bai, J. Wang, M. Wuttig, J. Li, N. Wang, A. P. Pyatakov, A. K. Zvezdin, L. E. Cross, and D. Viehland, *Applied Physics Letters* **86**, 032511 (2005).
- ²⁰ H. Béa, M. Bibes, S. Petit, J. Kreisel, and A. Barthélémy, *Philosophical Magazine Letters* **87**, 165 (2007).
- ²¹ D. Sando, A. Agbelele, D. Rahmedov, J. Liu, P. Rovillain, C. Toulouse, I. C. Infante, A. P. Pyatakov, S. Fusil, E. Jacquet, et al., *Nature Materials* **12**, 641 (2013), ISSN 1476-4660.
- ²² J. T. Heron, J. L. Bosse, Q. He, Y. Gao, M. Trassin, L. Ye, J. D. Clarkson, C. Wang, J. Liu, S. Salahuddin, et al., *Nature* **516**, 370 (2014), ISSN 1476-4687.
- ²³ S. Manipatruni, D. E. Nikonov, and I. A. Young, *Nature Physics* **14**, 338 (2018), ISSN 1745-2481.
- ²⁴ B. Prasad, Y.-L. Huang, R. V. Chopdekar, Z. Chen, J. Steffes, S. Das, Q. Li, M. Yang, C.-C. Lin, T. Gosavi, et al., *Advanced Materials* **32**, 2001943 (2020).
- ²⁵ Y. H. Chu, Q. Zhan, C.-H. Yang, M. P. Cruz, L. W. Martin, T. Zhao, P. Yu, R. Ramesh, P. T. Joseph, I. N. Lin, et al., *Applied Physics Letters* **92**, 102909 (2008).
- ²⁶ O. E. González-Vázquez, J. C. Wojdeł, O. Diéguez, and J. Íñiguez, *Phys. Rev. B* **85**, 064119 (2012).
- ²⁷ L. Zhang, Y.-L. Huang, G. Velarde, A. Ghosh, S. Pandya, D. Garcia, R. Ramesh, and L. W. Martin, *APL Materials* **7**, 111111 (2019).
- ²⁸ E. Parsonnet, Y.-L. Huang, T. Gosavi, A. Qualls, D. Nikonov, C.-C. Lin, I. Young, J. Bokor, L. W. Martin, and R. Ramesh, *Phys. Rev. Lett.* **125**, 067601 (2020).
- ²⁹ L. D. Landau, *Journal of Experimental and Theoretical Physics* **7**, 19 (1937).
- ³⁰ L. D. Landau, *Journal of Experimental and Theoretical Physics* **7**, 627 (1937).
- ³¹ A. Devonshire, *The London, Edinburgh, and Dublin Philosophical Magazine and Journal of Science* **40**, 1040 (1949).
- ³² A. Devonshire, *The London, Edinburgh, and Dublin Philosophical Magazine and Journal of Science* **42**, 1065 (1951).
- ³³ A. Umantsev, *Field Theoretic Method in Phase Transformations* (Springer New York, Dordrecht, Heidelberg, London, 2012).
- ³⁴ J.-M. T. K. M. Rabe, C. H. Ahn, *Physics of Ferroelectrics. A Modern Perspective* (Springer, Berlin, Heidelberg, 2007).
- ³⁵ P. Hohenberg and W. Kohn, *Phys. Rev.* **136**, B864 (1964).
- ³⁶ W. Kohn and L. J. Sham, *Phys. Rev.* **140**, A1133 (1965).
- ³⁷ G. Kresse and J. Furthmüller, *Phys. Rev. B* **54**, 11169 (1996).
- ³⁸ J. P. Perdew, A. Ruzsinszky, G. I. Csonka, O. A. Vydrov, G. E. Scuseria, L. A. Constantin, X. Zhou, and K. Burke, *Phys. Rev. Lett.* **100**, 136406 (2008).
- ³⁹ S. L. Dudarev, G. A. Botton, S. Y. Savrasov, C. J. Humphreys, and A. P. Sutton, *Phys. Rev. B* **57**, 1505 (1998).
- ⁴⁰ P. E. Blöchl, *Phys. Rev. B* **50**, 17953 (1994).
- ⁴¹ Y. Le Page and P. Saxe, *Phys. Rev. B* **65**, 104104 (2002).
- ⁴² P. Marton, A. Klíč, M. Paściak, and J. Hlinka, *Phys. Rev. B* **96**, 174110 (2017).
- ⁴³ H. Béa, B. Dupé, S. Fusil, R. Mattana, E. Jacquet, B. Warot-Fonrose, F. Wilhelm, A. Rogalev, S. Petit, V. Cros, et al., *Phys. Rev. Lett.* **102**, 217603 (2009).
- ⁴⁴ R. J. Zeches, M. D. Rossell, J. X. Zhang, A. J. Hatt, Q. He, C.-H. Yang, A. Kumar, C. H. Wang, A. Melville, C. Adamo, et al., *Science* **326**, 977 (2009).
- ⁴⁵ P. Chen, M. N. Grisolia, H. J. Zhao, O. E. González-Vázquez, L. Bellaiche, M. Bibes, B.-G. Liu, and J. Íñiguez, *Phys. Rev. B* **97**, 024113 (2018).